Journal of Solid State Chemistry 181 (2008) 1600–1608

Contents lists available at ScienceDirect

Journal of Solid State Chemistry

journal homepage: www.elsevier.com/locate/jssc

Controlling oriented aggregation using increasing reagent concentrations and trihalo acetic acid surfactants

Anthony S. Ratkovich, R. Lee Penn *

Department of Chemistry, University of Minnesota, 207 Pleasant St. S.E. Minneapolis, MN 55455, USA

ARTICLE INFO

Article history:
Received 25 January 2008
Received in revised form
19 March 2008
Accepted 28 March 2008
Available online 10 June 2008

Keywords:
Zinc oxide
Nanoparticle
Particle growth

ABSTRACT

Zinc oxide particle growth from homogenous solutions prepared with isopropyl alcohol was monitored using *in situ* UV–vis spectroscopy, and results show that the rate of ZnO particle growth and the final ZnO nanoparticle size depend strongly upon the concentrations of precursors and the identity of surfactants used. In addition, particle size versus time data was fit using the coarsening model and the simultaneous oriented aggregation and coarsening model in order to evaluate the effect of changing synthetic variables on the mechanism of nanoparticle growth. In general, an increase in growth by oriented aggregation with increasing precursor concentrations was observed, a result that was consistent with results from high-resolution transmission electron microscopy (HRTEM) characterization. The increase in precursor concentrations resulted in an increase in the number concentration of ZnO nanoparticles, which resulted in a higher probability of particle–particle interactions and hence increased growth by oriented aggregation. Additionally, particle growth in solutions of trifluoro-, trichloro-, and tribromoacetate surfactants was studied, and growth by oriented aggregation followed the trend expected based on the number concentration of zinc oxide particles. Growth with trifluoroacetate was an exception, with growth by oriented aggregation substantially suppressed.

1. Introduction

Nanosized ZnO has been suggested for use in many applications such as solar cells [1], sensors [2], and light-emitting diodes [3]. Solution phase synthesis of ZnO provides a low temperature, economical way to produce various ZnO nanostructures for incorporation into devices. Previous work has shown that ZnO particle size is strongly influenced by experimental conditions such as temperature [4], water concentration [5], anion [6], and solvent [7]. Understanding how these factors can be manipulated to control particle size, morphology, and surface composition is important for applying nanoscale ZnO in new and/or improved devices.

ZnO particle growth from homogenous solution proceeds by two major steps. First ZnO nanoparticles nucleate and grow until dissolved species drop to their saturation concentrations. Then, nanoparticle growth proceeds by two primary mechanisms, coarsening and aggregation. Coarsening involves growth of larger, more stable particles at the expense of smaller, less stable particles. Aggregation is growth by combination of particles into larger, secondary particles. Oriented aggregation (OA) is a special case of aggregation in which the secondary particles are composed of oriented primary building block particles [8,9,10]. Previously, coarsening and OA have been shown to operate simultaneously during particle growth from initially homogenous solvents [11,12] and initially homogenous solutions [13,14]. Improved understanding of the impact of solution conditions (i.e., surfactant and precursor concentrations) on particle growth is expected to enable development of methods to enhance or inhibit one growth mechanism or another [15]. An example of using OA for producing a specialized nanostructure was shown by Adachi et al. They determined that the efficiency of dye-sensitized solar cells was improved by exploiting the OA growth mechanism to synthesize single-crystal-like anatase nanowires, which lead to a high rate of electron transfer through the anatase nanonetwork [16]. Controlling OA also offers the potential to make single crystals with morphologies that defy symmetry, have relatively large size but also high surface area, and provide a mechanism for controllable defect concentrations.

In addition to understanding growth, controlling the composition of the nanoparticle surface is important for implementing nanoscale ZnO in new or improved devices. In particular, dye-sensitized solar cells can be constructed using nanosized ZnO particles with dye molecules adsorbed to their surfaces. Solar cells using this technology are potentially more efficient and cost effective than current solar cells designs [17]. Particles are usually

* Corresponding author. Fax: +1 612 626 7541.
E-mail address: rleepenn@umn.edu (R. Lee Penn).

0022-4596/$ - see front matter © 2008 Elsevier Inc. All rights reserved.
doi:10.1016/j.jssc.2008.03.042

synthesized and then subsequently sensitized with dye molecules such as the ruthenium complex, *cis*–bis (4,4′-dicarboxy-2,2′-bipyridine)-bis-(isothiocyanato)-ruthenium(II). The ability of the synthesized particles to become sensitized will depend upon their surface composition, which can be dependent upon surfactants used during synthesis. Understanding how the surfactant used in synthesis will impact the resulting ZnO nanostructure and the ability of the resulting nanostructure to become sensitized is important for improving dye-sensitized solar cell devices, and this is the focus of ongoing work.

2. Experimental

2.1. Materials

Reagents used in this study were zinc perchlorate hexahydrate (17–18% Zn complexometric), zinc acetate dihydrate (99.999%), sodium hydroxide (99%), isopropyl alcohol (IPA; 99.9%), tribromoacetic acid (TBAA; 99%), trichloroacetic acid (TCAA; 99.0%), trifluoroacetic acid (TFAA; 98%), and glacial acetic acid (AA; 99%). All chemicals were purchased from Aldrich Chemical Co. and used as received. All glassware used in reagent preparation was soaked overnight in 4 M nitric acid and rinsed with purified water, followed by a rinse with IPA. The quartz cuvettes used for *in situ* growth reactions were soaked for 24 h in concentrated oxalic acid, rinsed with milliQ water (18 MΩ cm, Millipore Corporation), and finally rinsed with IPA.

2.2. Reagent preparation

All solutions were prepared by dissolution of solids or combination of liquids in IPA at room temperature. In the case of the sodium hydroxide solution, it was heated to 65 °C for 3 h to speed dissolution. Surfactant solutions were neutralized by combining equimolar sodium hydroxide/IPA and surfactant/IPA solutions. Neutralization was performed in order to ensure careful control of Zn:OH. The total water content in the reactions was kept constant at approximately 0.040 M when using zinc perchlorate and 0.036 M when using zinc acetate. This accounts for water from the hydrated zinc precursor, water from neutralizing surfactants, and water found in isopropyl alcohol.

2.3. Particle synthesis: increasing zinc concentration

ZnO nanoparticles were synthesized from homogenous solutions of precursors using a modified version of the method from Bahnemann et al. [18,19]. Growth was monitored by *in situ* UV–vis spectroscopy. For these experiments, the concentrations of zinc acetate used were 0.5, 0.6, 0.75, 1.25, 1.5, 1.75, and 2.0 mM. The $[Zn^{2+}]$:$[OH^-]$ concentration ratio was kept constant at 0.625, and the reaction temperature used was 65 °C for all variable concentration reactions. Samples involving increased reagent concentrations are referred to by the concentration of zinc precursor used.

The balanced chemical equation for the nucleation reaction associated with this synthesis can be written as

$$Zn(C_2H_3O_2)_2 + 2NaOH \xrightarrow{IPA} ZnO(s) + H_2O + 2NaC_2H_3O_2. \quad (1)$$

The solution of sodium hydroxide in IPA was transferred to a quartz cuvette and brought to the desired reaction temperature. The reaction was initiated by injection of the zinc acetate solution into the cuvette, and the solution was vigorously stirred at all times using a Teflon-coated magnetic stir bar.

2.4. Particle synthesis using trihalo acetic acid surfactants

This synthesis was adapted from Bahnemann et al. [18,19] The balanced chemical equation for the nucleation reaction can be written as

$$Zn(ClO_4)_2 + 2NaOH \xrightarrow{IPA} ZnO(s) + H_2O + 2NaClO_4. \quad (2)$$

Appropriate volumes of the sodium hydroxide and surfactant solutions (in IPA) were transferred to a quartz cuvette and brought to the desired reaction temperature using the Peltier temperature controller. The reaction was initiated by injection of 1 mM zinc perchlorate solution into the cuvette, and the solution was vigorously stirred at all times using a Teflon-coated magnetic stir bar.

Four different surfactants were used to study the effects of surfactant identity on particle growth: acetic acid, trifluoroacetic acid, trichloroacetic acid, and tribromoacetic acid. The concentration of surfactant was kept constant at 0.35 mM. This concentration corresponds to approximately two monolayers of surface coverage on a 4 nm particle, assuming all Zn^{2+} reacted to form ZnO and using an estimate of four surface sites per square nanometer.

2.5. In situ UV–vis spectroscopy and particle size characterization

Particle growth was monitored *in situ* using an Agilent 8453 UV–vis spectrometer equipped with a Peltier temperature controller and magnetic stirrer. Each particle growth experiment was performed in a quartz cuvette fitted with a Teflon stopper to prevent solvent evaporation. In addition, atmospheric moisture affects reproducibility as water accumulates in stock solutions and reaction mixtures and causes variability in growth. Thus, solution preparation and particle growth were performed in a humidity-controlled environment, with relative humidity maintained at less than 10%. Absorbance spectra were acquired between 190 and 1200 nm every minute for the first 15 min, every 5 min for the next 45 min, and every 15 min through 6 h.

The average band gap for each sample was determined by finding the inflection point of the absorption edge using the second derivative of each UV–vis spectrum. The effective mass model was employed to calculate the average particle size from the average band gap using $\varepsilon = 8.5$, $m_e = 0.26$, $m_h = 0.59$, and $E_g^{bulk} = 3.2$ eV. Owing to the relatively small effective masses for ZnO, quantum size effects are expected to occur for particles sizes up to ~8 nm [20,21]. The tight binding model was also employed to calculate the average particle size from the average band gap in order to compare the two models [22]. Average experimental sizes were calculated using a minimum of three trials per specified condition, and the experimental error discussed is the experimental uncertainty determined at the 95% confidence interval for the sample. The average experimental uncertainty in the average band gap for the concentration study is 0.007 eV, which corresponds to 0.05 nm as calculated using the effective mass model. The average experimental uncertainty in the average band gap for the surfactant study is 0.008 eV, which corresponds to 0.09 nm as calculated using the effective mass model. The experimental uncertainty reflects the high reproducibility of the experiments performed and not the error associated with employing the effective mass and the tight binding models for determining average particle size.

2.6. Characterization by high-resolution transmission electron microscopy (HRTEM)

Samples were prepared for HRTEM by dipping a 3 mm copper HRTEM grid coated with holey carbon film (SPI Supplies) into the

reaction mixture at the appropriate time. The resulting grid was then allowed to air dry in the humidity-controlled environment. Samples were examined using an FEI Tecnai F30 FEGTEM. Images were collected using a charge-coupled device (CCD) camera and analyzed using Gatan Digital Micrograph software.

3. Results and discussion

3.1. Growth as a function of relative zinc concentration

It has been previously shown that coarsening kinetics are independent of the zinc acetate concentration between 0.5 and 1.25 mM for the Zn:OH concentration ratio of 0.625 [23]. In contrast, results obtained via *in situ* UV–vis spectroscopy to acquire reproducible data at the early stages particle growth shows that ZnO growth kinetics are strongly dependent upon zinc acetate concentration using a Zn:OH concentration ratio of 0.625 (Figs. 1 and 2). Here, we employ both the effective mass model and the tight binding model to calculate average particle size from the average band gap determined from the UV–vis spectra. Recent work has shown that the effective mass model overestimates particle size and that the tight binding model may be more suitable for calculating particle size [24]. Both models were included here for facile comparison to previously reported results [11]. Final particle sizes, particle concentration, and growth rate constants show systematic trends as the reagent concentrations, hydroxide and zinc acetate, are changed while maintaining their molar ratios, and, while the sizes determined do vary, the trends observed are consistent between models.

Fig. 2 shows particle size, as determined by *in situ* UV–vis spectroscopy, versus time for experiments using a zinc acetate concentration ranging from 0.5 to 2.0 mM with a Zn:OH concentration ratio 0.625. The inset shows the particle size at 5 min versus zinc acetate concentration. In addition, the final particle size also increases with zinc acetate concentration although the spread is rather narrow, only ~0.7 nm variation when comparing final sizes from experiments using 0.75–2.0 mM zinc acetate. Also, as the reagent concentrations are increased the ZnO particle concentration increases, which is as expected and can be seen by the difference in the maximum absorbance of Fig. 1A ($[Zn^{2+}] = 0.5$) and Fig. 1B ($[Zn^{2+}] = 2.0$). Finally, particle

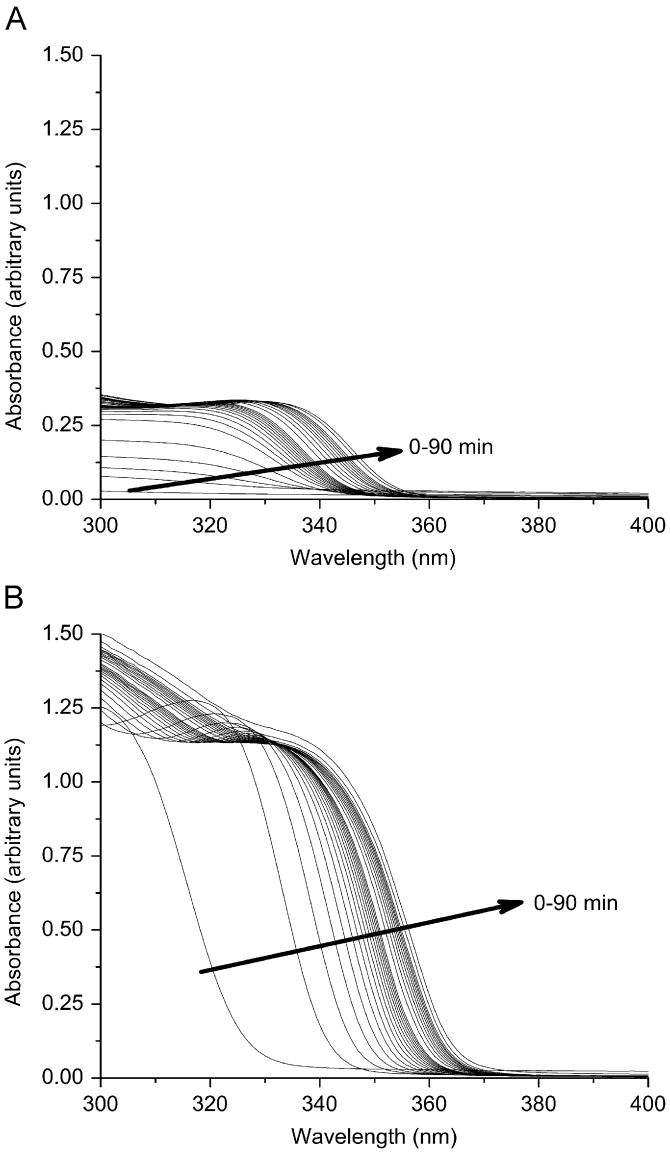

Fig. 1. *In situ* UV–vis spectra for 0.5 (A) and 2.0 (B) mM $Zn(acetate)_2$ as a function of time after initiation of the reaction. Reactions were performed at 65 °C and using 0.625 Zn:OH.

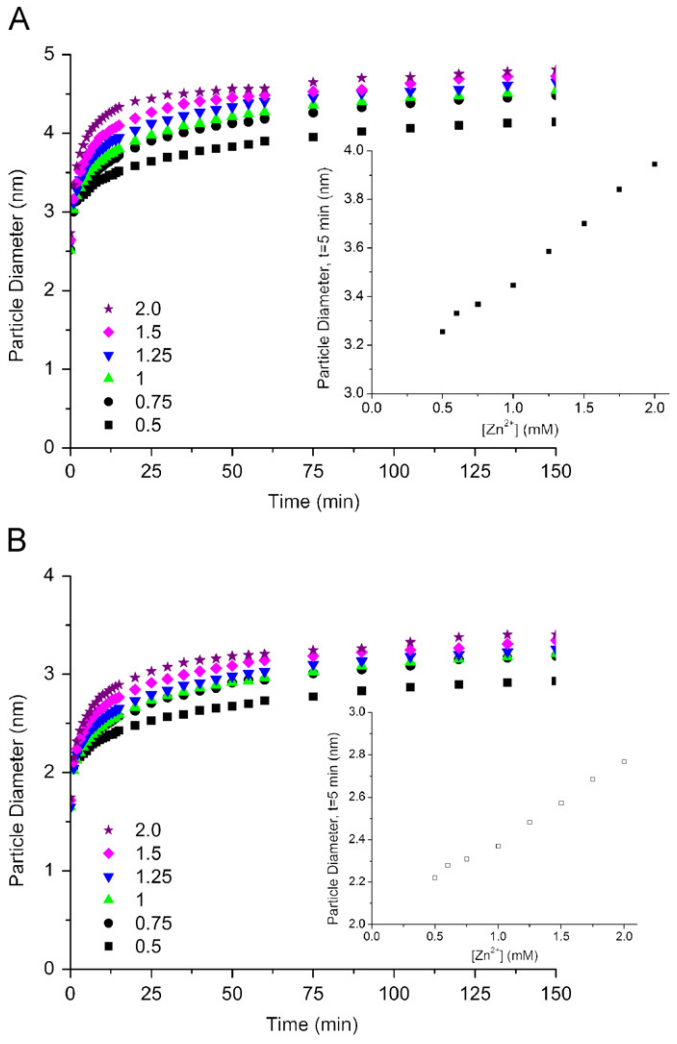

Fig. 2. Particle size versus time as a function of increasing $Zn(acetate)_2$ concentration (listed in the legend using units of nM Zn^{2+}). Particle sizes were calculated using the (A) effective mass model and (B) tight binding model. The inset on each graph shows the particle size at 5 min as a function of initial zinc concentration. Reactions were performed at 65 °C using a 0.625 Zn:OH.

Table 1
Particle sizes and estimates of OA% as determine from calibrated HRTEM images (ca. 200 particles per sample)

Zinc acetate (mM)	Time (min)	UV–vis particle size EMM/TB (nm)	HRTEM particle size (nm)	Min. estimate OA%	Max. estimate OA%
0.5	5	3.3/2.2	3.3	0.5	0.6
0.5	10	3.4/2.4	3.3	0.6	0.9
0.5	25	3.6/2.5	3.5	0.5	0.7
0.5	120	4.1/2.9	4.0	0.6	0.8
2.0	5	4.0/2.8	3.8	11.0	15.5
2.0	10	4.2/3.0	4.1	10.8	16.7
2.0	25	4.4/3.2	4.3	11.7	15.7
2.0	120	4.8/3.5	4.7	10.6	14.1

sizes determined using UV–vis spectroscopy agree well with particle sizes determined from HRTEM, as can be seen in Table 1. The calculations of particle size using either the effective mass or tight binding models are sensitive to the value used for the bulk band gap of zinc oxide (3.2–3.4 eV [25,26]); thus, it is important that a complementary technique is used to verify that the particle sizes calculated are reasonable.

The rate constant for growth by coarsening, k_c, was determined as a function of increasing reagent concentration fitting experimental data using the classic coarsening model (Eq. (3)) [27]. This model describes growth solely by coarsening, and D_t is the particle diameter at time t, D_0 is the particle diameter at time zero, t is time, k_c is the growth rate

$$D_t = D_0 + k_c t^{1/n} \quad (3)$$

constant, and n is a parameter that describes the coarsening mechanism for the system. The parameter $n = 3$ results in the best fits, indicating that the primary mechanism for growth by coarsening is diffusion limited coarsening, which is consistent with Pesika et al. [17] and Talapin et al. [28]. The growth rate constant, k_c, as determined using both the effective mass and the tight binding models, increases as the zinc concentration increases (Fig. 3). The largest increase is observed between 0.5 and 0.75 mM zinc acetate, after which the increase is less pronounced. This increase is likely due to the change in the rate of saturation as a function of zinc concentration. Saturation occurs when the absorbance onset reaches a constant maximum some point after the reaction is initiated. The slowest saturation is observed at the 0.5 mM concentration, with saturation occurring between 5 and 6 min. Saturation occurs between 1 and 2 min for the 0.6–0.75 mM samples and between the 0 and 1 min sample for the 1.0–1.5 mM concentrations. Saturation occurs prior to acquisition of the first UV–vis spectrum (the "0 min sample", which is collected 7–10 s after injection) for the 1.75 and 2.0 mM concentrations. Slow saturation results in slower growth by coarsening, and fast saturation results in faster growth by coarsening.

The growth rate associated with OA increases as a function of increasing zinc acetate concentration. Fig. 4 shows representative HRTEM images of ZnO nanoparticles produced using low (0.5 mM Zn^{2+}; Figs. 4A and B) and high (2 mM Zn^{2+}; Figs. 4C and D) reagent concentrations. Lattice fringes and paticles sizes were measured from the calibrated HRTEM images, and in all cases, the lattice fringe spacings were consistent with zinc oxide with the wurtzite structure ($a = 3.25$ Å, $c = 5.21$). In general, most ZnO nanocrystals appeared to be spherically shaped. However, more particles with morphologies consistent with OA were observed with increasing reagent concentration, and these results are summarized in Table 1. Minimum estimates for the percentage of particles with morphologies consistent with OA were determined by counting the number of obvious oriented aggregates with visible lattice fringes divided by the total number of particles in the HRTEM image (with or without lattice fringes). Maximum estimates were determined by dividing the total number of oriented aggregates with visible lattice fringes by the total number of particles with visible lattice fringes.

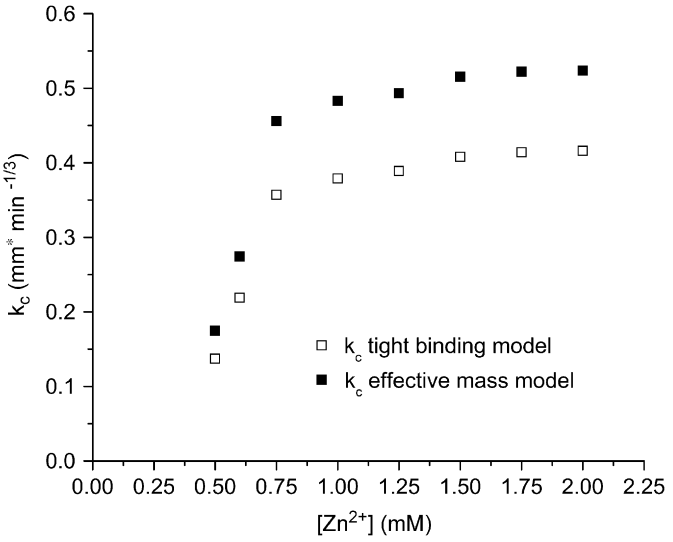

Fig. 3. Coarsening growth rate constant, k_c, as a function of increasing zinc acetate concentration.

Growth by OA was also evaluated by fitting the growth data using the simultaneous coarsening and OA model proposed by Huang et al. (Eq. (4)) [9]. Here D_t is the

$$D_t = \frac{D_0(\sqrt[3]{2}k_1 t + 1)}{(k_1 t + 1)} + k_2 t^{1/n} \quad (4)$$

particle diameter at time t, D_0 the diameter at time zero, k_1 the rate constant for oriented aggregation, k_2 the rate constant for simultaneous coarsening and OA, n the parameter describing the mechanism limiting particle growth, and t time. In general, this model predicts that growth is initially dominated by OA resulting in very fast growth early in the reaction. As the reaction proceeds, growth by coarsening becomes the more dominant mechanism. The growth rate constants, k_1 and k_2, were determined using both the effective mass and tight binding models and are shown in Fig. 5 versus zinc precursor concentration. Both k_1 and k_2 increase as a function of the initial zinc concentration. The rate constant for growth by simultaneous coarsening and OA, k_2, shows similar behavior when compared with rate constant for growth by coarsening, k_c (discussed above). The change in k_2 can be explained in a similar manner as with k_c because k_2 describes growth dominated by coarsening. Both, the growth rate constant for OA, k_1, and the ZnO particle number concentration at 5 min ($[\sharp ZnO]_{5\,min}$) increase as a function of zinc concentration, as shown in Fig. 5A. An effective ZnO particle concentration can be calculated from the maximum absorbance and an extinction coefficient of 605 L/mol cm [23] and then used to calculate $[\sharp ZnO]_{5\,min}$, by using the average ZnO particle size at 5 min and an assumption of spherical morphology. The increase in k_1 as a function of $[\sharp ZnO]_{5\,min}$ is consistent with an increase in the probability of particle–particle interactions. With particle–particle interactions dramatically increased, OA% and thus k_1 are both expected to increase, as observed.

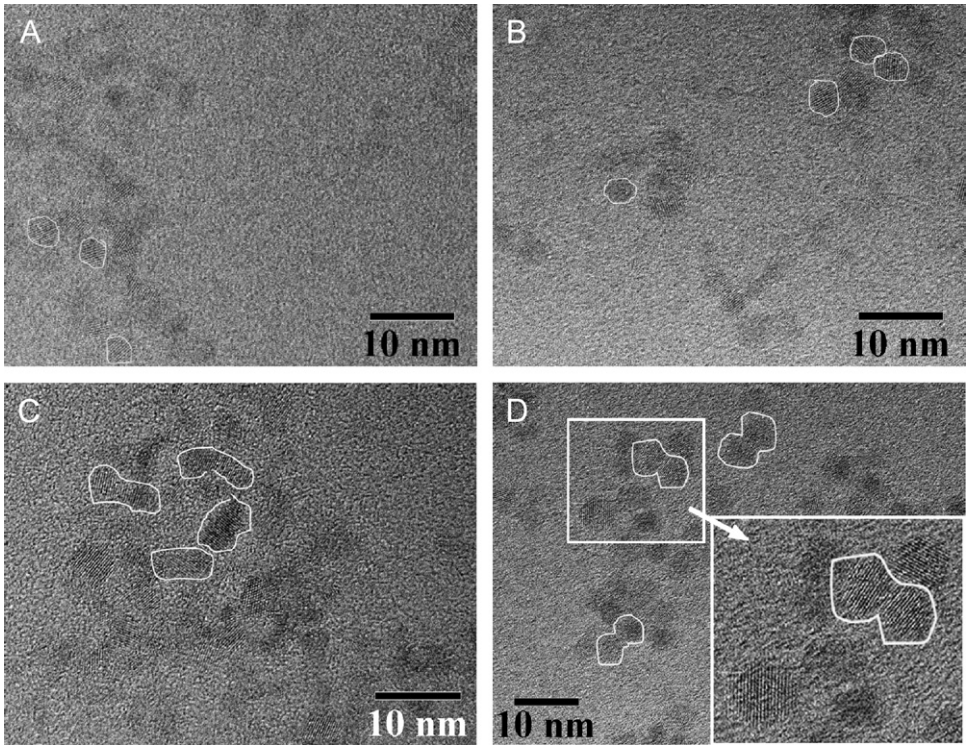

Fig. 4. Representative HRTEM images for ZnO particles using 0.5 mM zinc acetate at 5 min (A) and 120 min (B) and 2.0 mM zinc acetate at 10 min (C) and 120 min (D). The average particle sizes obtained from counting 150 particles for each sample are shown in Table 1. Examples of primary nanocrystals and oriented aggregates are outlined in A and B, and examples of oriented aggregates are outlined in C and D. Lattice fringes in calibrated HRTEM images were measured and were consistent with zinc oxide with the wurtzite structure ($a = 3.25$ Å, $c = 5.21$). Close up of an oriented aggregate (E).

3.2. Particle growth with added surfactant

Coarsening and OA growth kinetics for ZnO nanoparticle growth from solutions containing the surfactants acetate, trifluoroacetate, trichloroacetate, and tribromoacetate were evaluated using the two growth models described above. Results demonstrate that the particle growth depends strongly upon the identity and concentration surfactant employed (Fig. 6). Particle sizes were calculated using the effective mass and tight binding models, and the rate constants for growth determined showed some variation in magnitude with the overall trends remaining consistent. The rate constant for coarsening, k_c, was determined for each experiment using the classic coarsening model (Eq. (1)) as described above. Fig. 7 shows the rate constant for coarsening, k_c, plotted versus the increasing size of the halogen. The resulting trends show that the larger the halogen on the surfactant, the smaller the growth rate constant, k_c (Fig. 7) and the smaller the final particle size (Fig. 6).

The growth rate constants, k_1 and k_2 were also determined for each of the experiments using the OA and coarsening model (Fig. 8). As expected, the growth rate constant, k_2, shows the same trend as k_c and can be explained similarly (Fig. 8B). In contrast, the growth rate constant for oriented aggregation, k_1, decreases as the size of the halogen decreases (Fig. 8A). In addition, the analysis of the HRTEM images show decreased OA as the size of the halogen decreases (Table 2). At first glance, this data can be interpreted to mean that the trhihaloacetates suppress growth by OA. However, the variation in growth by OA% follows the trend expected for increasing ZnO number concentration. Fig. 9 shows the log of k_1 versus the log of $[\sharp ZnO]_{5\,min}$ for both the concentration (closed squares, bold line) and the surfactant (closed circles, dashed line) series. As in the case of the concentration series, k_1 increases as a function of increasing $[\sharp ZnO)]_{5\,min}$ for growth using AA, TCAA, and TBAA. The dashed line is parallel to the bold line, which represents the least-squares fit to the concentration series. The overall differences in these two datasets is attributable to experimental differences most importantly the differences in water concentration (2.3 mM H_2O in the surfactant series and 6.3 mM H_2O for the concentration series at 1 mM Zn^{2+}), overall surfactant concentration (2 mM for the concentration series and 0.3474 mM for the surfactant series), and the particle sizes at $t = 5$ min (sizes were approximately 1 nm smaller for the concentration series than for the surfactant series). In fact, a drop in the rate of growth by OA for larger particles is consistent with previous results, which showed an order of magnitude decrease in the second-order rate constant for oriented aggregation for a 1 nm increase in iron oxide nanoparticle size in the 3–7 nm size range [29]. Thus, we conclude that the effect of using AA and the trihaloacetates TCAA and TBAA follows the trend of increasing OA% with increasing $[\sharp ZnO]_{5\,min}$.

The rate constant for growth by OA% with TFAA, on the other hand, falls far below the dashed line (Fig. 9), which represents the expected relationship between k_1 and $[\sharp ZnO]_{5\,min}$. Thus, we conclude that TFAA strongly inhibits nanoparticle growth by OA, a conclusion that is also supported by HRTEM results (Table 2). Overall, there are two plausible possibilities for why adsorption of TFAA might inhibit growth by OA%. The first is the possibility of a difference in the strength of binding of the surfactant molecules to the ZnO surface, since those molecules must be removed from the interface between two primary ZnO nanoparticles in order for the oriented aggregate to form. The second possibility is suppression of particle–particle interactions. The adsorption of the TFAA molecules is expected to produce a shell of negative charge around the ZnO nanoparticle as a consequence of the high electronegativity of the fluorine atom. Such a negatively charged shell would be expected to decrease particle–particle interactions

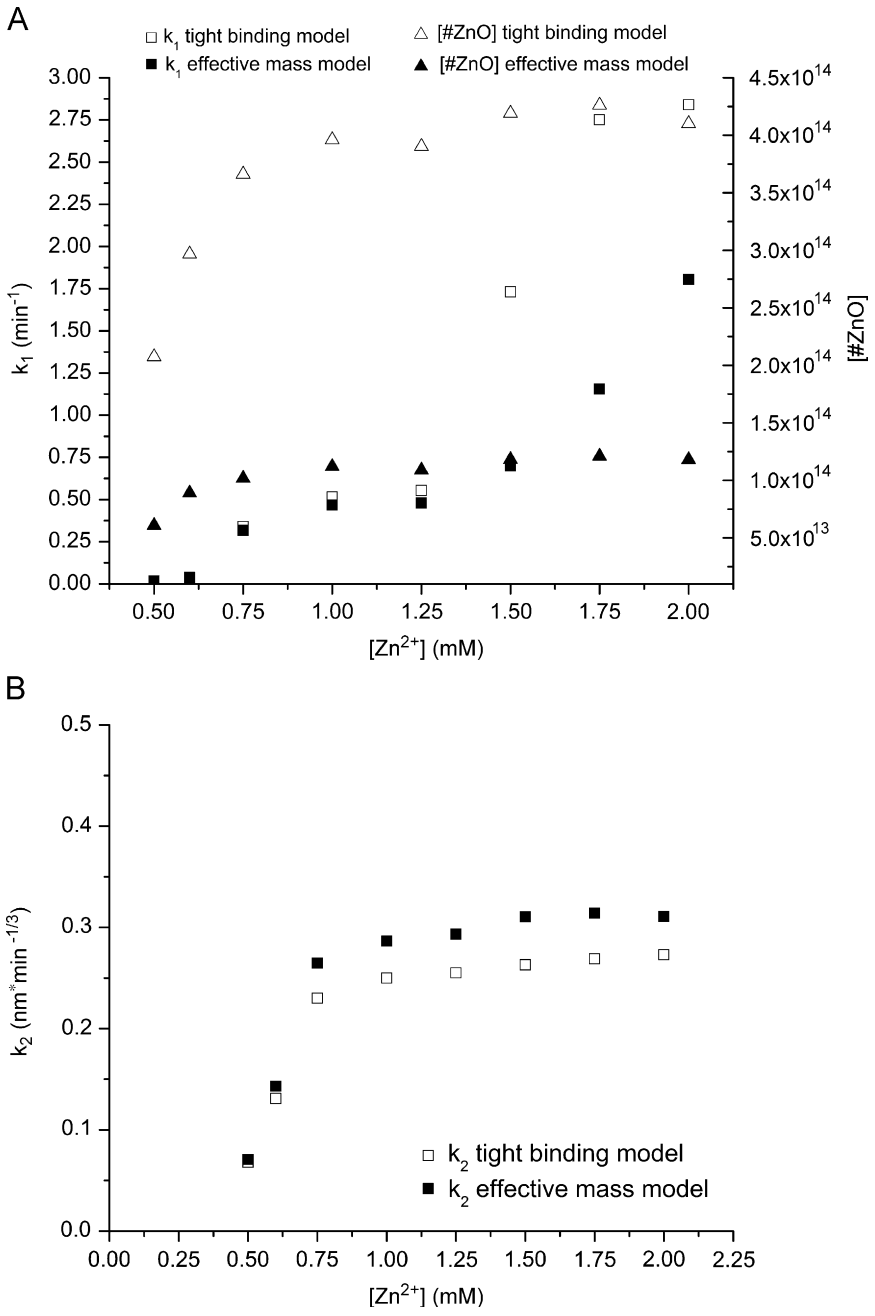

Fig. 5. (A) Growth rate constant k_1 and ZnO particle number concentration as a function of initial zinc precursor concentration for the effective mass model (closed squares and triangles) and the tight binding model (open circles and triangles). (B) k_2 as a function of zinc precursor concentration for the effective mass model (closed squares) and the tight binding model (open squares).

by way of electrostatic repulsion, which would inhibit growth by OA.

The dependence of $\log k_1$ on particle size at constant concentration shows that as particle size decreases $\log k_1$ increases. This agrees with previous work that shows increasing OA rate as size decreases [29]. The black lines in Fig. 10 contain values for log k_1 that were determined from growth reactions using 1 mM of zinc precursor. When the zinc precursor concentration increases, $\log k_1$ increases even as particle size increases, contrary to the expected trend. We conclude that the effect of the increased number concentration of ZnO nanoparticles has a much stronger effect than does the changing particle size for these conditions. Overall, these results show that modifying solution conditions can be used to increase OA, even at larger particle sizes, which could be useful when engineering specialized nanostructures composed of specific sized primary building blocks.

4. Conclusions

Zinc oxide particle growth has been shown to be affected by both zinc precursor concentration and surfactant. Particle growth as a function of zinc concentration was shown to increase growth by coarsening due to the variation in saturation rate when using different concentrations of zinc acetate but maintaining the Zn:OH molar ratio. Growth by OA was also shown to increase as a function of zinc concentration as a consequence of higher particle concentration, which leads more particle–particle

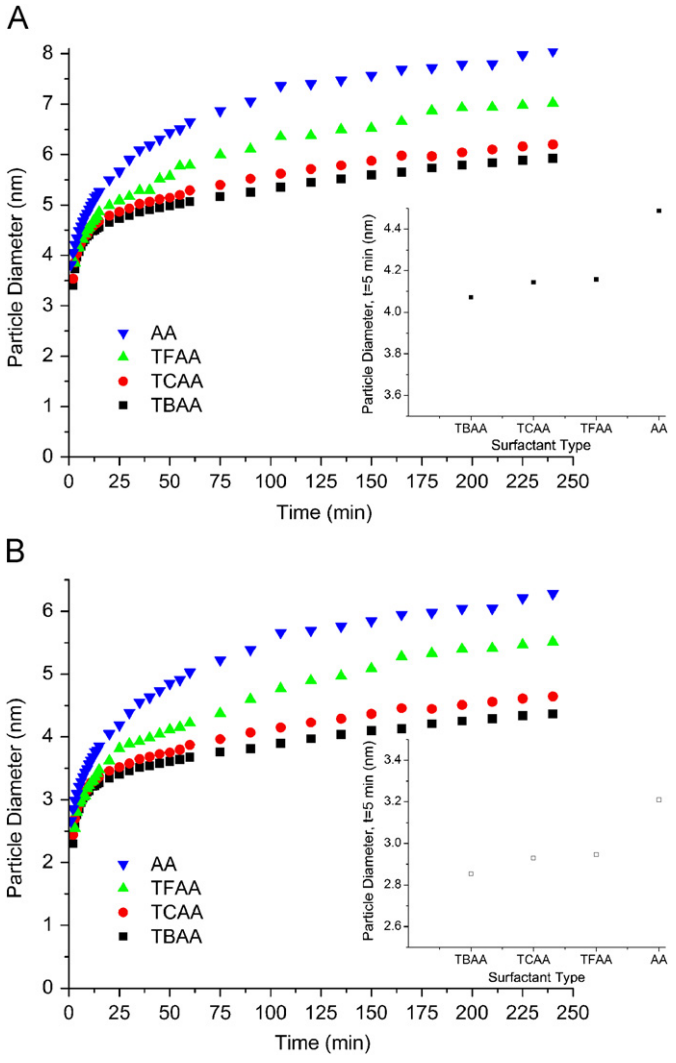

Fig. 6. Particle diameter versus time for growth as a function of surfactant with particle sizes calculated using the effective mass model (A) and the tight binding model (B). Reactions were performed at 65 °C and using 1 mM Zn^{2+} and 0.625 Zn:OH.

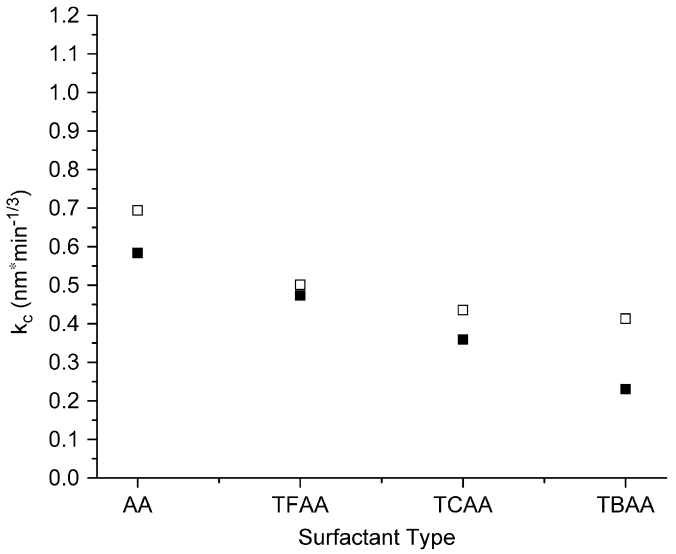

Fig. 7. Growth rate constant k_c as a function of trihalo acetic acid surfactants with particle sizes calculated using the effective mass model (closed squares) and the tight binding model (open squares).

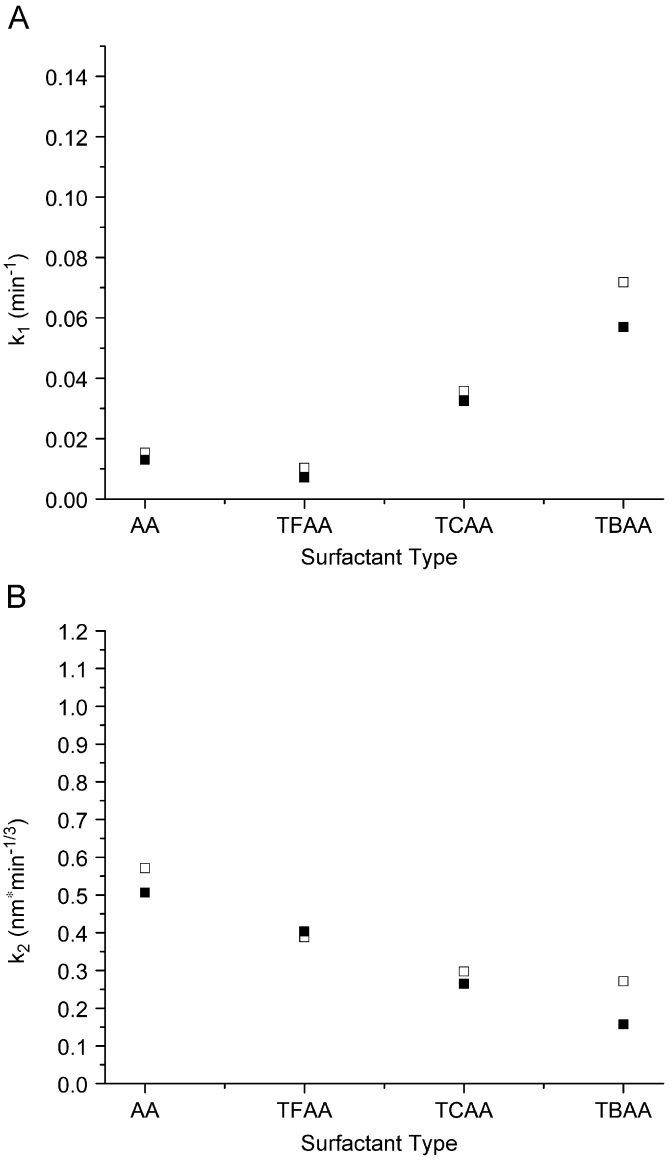

Fig. 8. Growth rate constants k_1 (A) and k_2 (B) as a function of trihalo acetic acid surfactants. Particle sizes were calculated using the effective mass model (closed squares) and the tight binding model (open squares).

Table 2
HRTEM results for ZnO particle growth as a function of trihalo acetic acid surfactants

Surfactant	Time (min)	Min. estimate OA%	Max. estimate OA%
TBAA	15	8.4	15.4
TBAA	120	7.9	15.0
TCAA	15	8.6	14.6
TCAA	120	7.7	13.7
TFAA	15	1.0	2.1
TFAA	120	1.4	2.9
AA	15	1.7	3.4
AA	120	2.0	3.6

interactions, and, hence increased growth by OA. When trihaloacetates are used during ZnO nanoparticle growth, a similar relationship between the rate of growth by OA and the number concentration of ZnO nanoparticles was observed as for the experiments varying the Zn^{2+} concentration while maintaining the molar ratios of the reagents (i.e., hydroxide and Zn^{2+}). The case

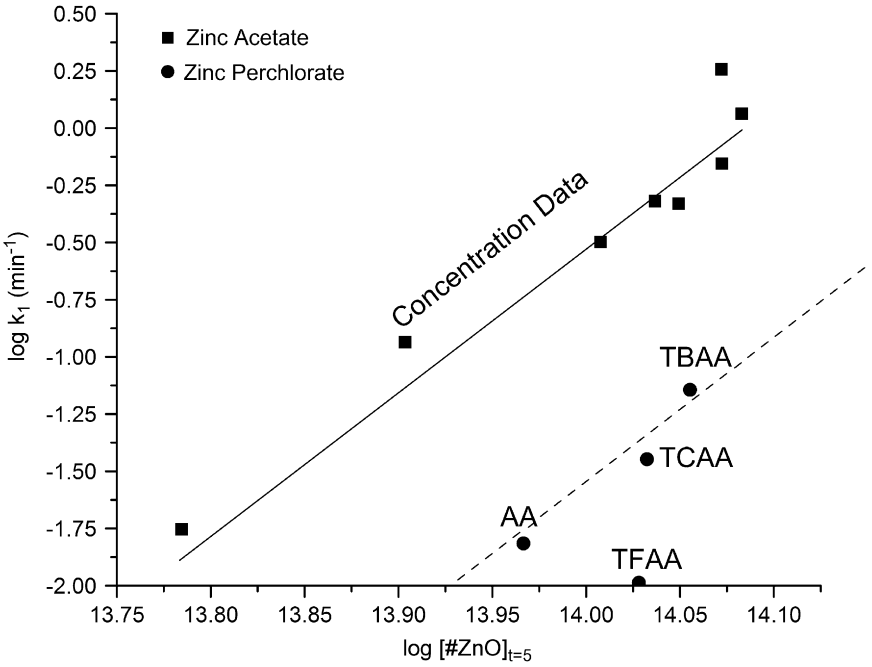

Fig. 9. Log of the rate constant k_1 versus log of the number concentration of ZnO nanoparticles at $t = 5$ min ($[ZnO]_{5\,min}$) for increasing concentration growth data (closed squares) and surfactant growth data (closed circles). The line is a least-squares fit to the concentration data and was translated over the surfactant data to highlight the TFAA case.

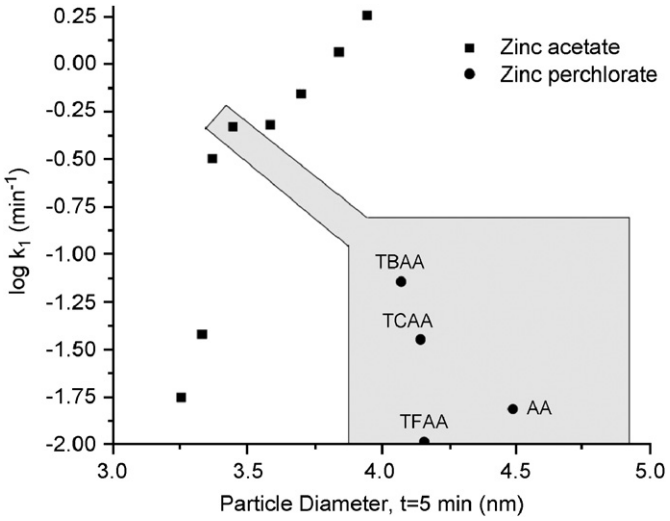

Fig. 10. Log of k_1 as a function of particle diameter at 5 min (nm). Points contained within the shaded region are reactions performed using 1 mM zinc precursor and are highlighted to show size effect and surfactant suppression effect.

of growth with TFAA was the exception, for which substantial inhibition of growth by OA was observed. Because the coarsening growth rate constant did not exhibit a similar decrease in magnitude, we conclude that the strength of TFAA binding to the ZnO nanoparticle surface is similar as for acetate. However, adsorption of the TFAA molecule, with the increased electronegativity of the fluorine atom, is expected to result in the formation of a negatively charged shell on the ZnO nanoparticles, which would suppress particle–particle interactions by way of electrostatic repulsions and, hence, suppress growth by OA. Overall, results show that primary route by which growth by OA can be enhanced is by increasing the number concentration of ZnO nanoparticles at the early stages of growth, which can be accomplished by simply increasing the precursor concentrations. Furthermore, growth by OA can be inhibited by employing an appropriate surfactant, such as trifluoroacetate, as used in this work.

Acknowledgments

We acknowledge the National Science Foundation (Career-036385 and MRI EAR-0320641) and the University of Minnesota for funding. Parts of this work were carried out in the University of Minnesota I.T. Characterization Facility, which receives partial support from NSF through the NNIN program.

References

[1] B. O' Regan, M. Gratzel, Nature 353 (1991) 737.
[2] M. Yang, D. Wang, L. Peng, Q. Zhao, Y. Lin, X. Wei, Sensor. Actuat. B 117 (2006) 80–85;
C. Rout, A. Raju, A. Govindaraj, C. Rao, Solid State Commun. (2006) 136–138.
[3] V. Colvin, M. Schlamp, A. Alivisatos, Nature 370 (1994) 354.
[4] E. Wong, J. Bonevich, P. Searson, J. Phys. Chem. B 102 (1998) 7770–7775.
[5] Z. Hu, D. Escamilla Ramirez, B. Heredia Cervera, G. Oskam, P. Searson, J. Phys. Chem. B 109 (2005) 11209–11214.
[6] Z. Hu, G. Oskam, R. Penn, N. Pesika, P. Searson, J. Phys. Chem. B 107 (2003) 3124–3130.
[7] Z. Hu, G. Oskam, P. Searson, J. Colloid Interf. Sci. 263 (2003) 454–460.
[8] R. Penn, J. Phys. Chem. B 108 (2004) 12707–12712.
[9] J.F. Banfield, R.L. Penn, Science 281 (1998) 969–971.
[10] R.L. Penn, J.F. Banfield, Am. Min. 83 (1998) 1077–1082.
[11] H. Huang, H. Zhang, J. Banfield, J. Phys. Chem. B 107 (38) (2003) 10470–10475.
[12] S.L. Isley, R.L. Penn, J. Phys. Chem. C 112 (2008) 4469–4474.
[13] A. Ratkovich, R. Penn, J. Phys. Chem. C 111 (2007) 14098–14104.
[14] C. Pacholski, A. Kornowski, H. Weller, Angew. Chem. Int. Ed. 41 (2002) 1188.
[15] J. Polleux, N. Pinna, M. Antonietti, C. Hess, U. Wild, R. Schlçgl, M. Niederberger, Chem. Eur. J. 11 (2005) 3541–3551.
[16] M. Adachi, Y. Murata, J. Takao, J. Jiu, M. Sakamoto, F. Wang, J. Am. Chem. Soc. 126 (2004) 14943–14949.
[17] K. Westermark, H. Rensmo, H. Siegbahn, K. Keis, A. Hagfeldt, L. Ojamae, P. Persson, J. Phys. Chem. B 106 (2002) 10102–10107.
[18] D. Bahnemann, C. Kormann, R. Hoffmann, J. Phys. Chem. 91 (1987) 3789.
[19] E. Meulenkamp, J. Phys. Chem. B 102 (1998) 5566–5572.
[20] L. Brus, J. Phys. Chem. B 90 (1986) 2555.
[21] N. Pesika, K. Stebe, P. Searson, J. Phys. Chem. B 107 (2003) 10412–10415.
[22] R. Viswanatha, S. Sapra, B. Satpati, P. Satyam, B. Dev, D. Sarma, J. Mater. Chem. 14 (2004) 661–668.

[23] Z. Hu, J. Herrera Santos, G. Oskam, P. Searson, J. Colloid Interf. Sci. 288 (2005) 313–316.
[24] R. Viswanatha, H. Amenitsch, D. Sarma, J. Am. Chem. Soc. 129 (2007) 4470–4475.
[25] L. Solymar, D. Walsh, Electrical Properties of Materials, sixth ed, Oxford University Press, Oxford, 1999, p. 138.
[26] A. West, Basic Solid State Chemistry, second ed, Wiley, New York, 1999, p. 118.
[27] J. Banfield, H. Zhang, Rev. Mineral Geochem. 44 (2001) 1–58.
[28] D. Talapin, A. Rogach, M. Haase, H. Weller, J. Phys. Chem. B 105 (2001) 12278–12285.
[29] R. Penn, K. Tanaka, J. Erbs, J. Cryst. Growth 309 (2007) 97–102.